Novel FBG-Based Effective Stress Cell for Direct Measurement of Effective Stress in Saturated Soil

Jian-Hua Yin[1]; Jie-Qiong Qin[2]; and Wei-Qiang Feng, Ph.D.[3]

Abstract: In this study, a novel effective stress cell based on fiber Bragg grating (FBG) sensing technology is developed for direct measurement of effective stress in saturated soil. The primary concept of direct measurement is that the pore-water pressures acting on both front and back surfaces of the sensing plate do not induce the deflection of the sensing plate, and thus the measured deflection of the sensing plate is caused by the effective stress only. The calibration results of the FBG-based effective stress cell (FBG-ESC) demonstrate a good linearity between the Bragg wavelength of the FBG sensor and the applied pressure. The workability and performance of the FBG-ESC in a saturated soil have been verified in a physical model test subjected to vertical pressures. It is found that the effective stress data directly measured by the FBG-ESC agree well with the effective stress values calculated, according to the effective stress principle, from the difference between the total stress and pore-water pressure measured by conventional transducers. All these results indicate that the novel FBG-ESC is capable of directly measuring the effective stress in a saturated soil. **DOI: 10.1061/(ASCE)GM.1943-5622.0001724**.

Author keywords: Fiber optic sensor; FBG; Effective stress cell; Pore-water pressure; Total stress; Soil.

Introduction

Both deformation and stability are directly related to the effective stresses in soils (Terzaghi 1943; Lade and De Boer 1997; Rojas et al. 2017; Zhou et al. 2018). Effective stress is an important and fundamental variable for determining the deformation and stability of geotechnical structures. Therefore, determination of the effective stress plays a vital role in safety and stability assessments of geotechnical structures. According to the effective stress principle (Terzaghi 1943; Skempton 1960), the equilibrium of all forces in vertical direction in a cubic element can be expressed as

$$\frac{P}{A}=\frac{\sum N'}{A}+u \tag{1a}$$

$$\sigma=\sigma'+u \tag{1b}$$

$$\sigma'=\sigma-u \tag{1c}$$

where P = the total external vertical force on a cubic element (N); $\sum N'$ = summation of all vertical fractions of particle contact forces (N); A = the gross cross-sectional area of the cubic element (m^2); and u = the pore-water pressure in voids (Pa). In Eq. (1*b*), the total stress is $\sigma=P/A$ (Pa) and the effective stress σ' is defined as

$$\sigma'=\frac{\sum N'}{A} \tag{2}$$

Here, the effective stress σ' is defined as the average value of all vertical (normal) fractions of particle contact forces over the cubic element cross-section area (Pa). The normal way to determine this effective stress is to measure the pore-water pressure u and the total stress σ separately so that the effective stress can be calculated using Eq. (1*c*). In this study, we call this method using Eq. (1*c*) an indirect measurement method. Using this method, we need two separate transducers, one for measuring pore-water pressure and one for measuring the total stress, that is, σ as shown in Fig. 1(a) (Yin 2013). The elements in Fig. 1(a) are (1) a total earth pressure cell including one FBG sensor (FBG 1) used to measure the flexural strain adhered on the back of diaphragm and one FBG 2 for temperature measurement and compensation, and (2) a pore-water pressure cell in which FBG 3 is used to measure pore-water pressure. In fact, various types of transducers can be utilized for total stress measurement, including diaphragm-type transducers (Clayton and Bica 1993; Chang et al. 2000) and transducers based on null sensing technology (Talesnick 2013), dual L-shaped levers (Li et al. 2013), and a cantilever beam (Wei et al. 2018). The pore-water pressure can also be measured by other traditional transducers using strain gauges or newly developed technologies (Feng et al. 2016). These two separate elements are connected in a series. All these are for indirect measurement of effective stress.

Correia et al. (2009) developed an FBG-based effective soil pressure sensor by using two diaphragms as sensing elements for independent measurement of the total stress and pore-water pressure separately as shown in Fig. 1(b). The "effective soil pressure sensor" presented by Correia et al. (2009) used two diaphragms (Diaphragm A and Diaphragm B) shown in Fig. 1(b) as sensing diaphragms: Diaphragm A was used to measure the soil total stress and Diaphragm B was used to measure pore pressure. It is noted that both Diaphragm A and Diaphragm B were integrated as one big cell and FBGs were used as sensing elements. But,

[1]Chair Professor of Soil Mechanics, Dept. of Civil and Environmental Engineering, Hong Kong Polytechnic Univ., Hung Hom, Kowloon, Hong Kong, China (corresponding author). ORCID: https://orcid.org/0000-0002-7200-3695. Email: cejhyin@polyu.edu.hk

[2]Ph.D. Candidate, Dept. of Civil and Environmental Engineering, Hong Kong Polytechnic Univ., Hung Hom, Kowloon, Hong Kong, China.

[3]Assistant Professor, Department of Ocean Sciences and Engineering, The Southern University of Science and Technology, Shenzhen, Guangdong, China; formerly, Post-doctoral Fellow, Dept. of Civil and Environmental Engineering, Hong Kong Polytechnic Univ., Hung Hom, Kowloon, Hong Kong, China. Email: fengweiqiang2015@gmail.com.

Note. This manuscript was submitted on February 17, 2019; approved on January 16, 2020; published online on May 20, 2020. Discussion period open until October 20, 2020; separate discussions must be submitted for individual papers. This paper is part of the ***International Journal of Geomechanics***, © ASCE, ISSN 1532-3641.

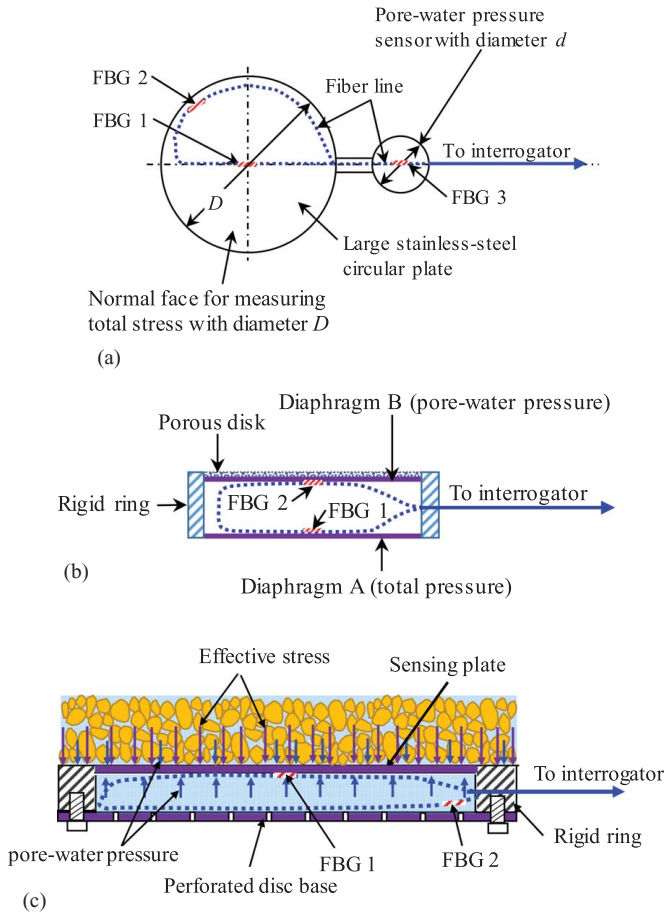

Fig. 1. Approaches to determination of effective stress: (a) an FBG-based transducer with two separate elements to measure pore-water pressure and total stress independently (plan view); (b) an FBG-based effective soil pressure sensor to measure pore-water pressure and total stress simultaneously (section view); and (c) our novel FBG-based effective stress cell using one diaphragm with pore-water pressure balanced (section view).

they still used Eq. (1*c*) to calculate the effective stress of soil. Therefore, this method by Correia et al. (2009) is still an indirect measurement method.

In this study, we present a novel FBG-based effective stress cell for direct measurement of effective stress in saturated soil using only one diaphragm without measuring pore-water pressure. This new FBG-based effective stress cell has been validated through a physical model test and comparison with data from an indirect measurement method.

Working Principle and Design of a Novel FBG-Based Effective Stress Cell

Fiber Bragg grating, as a widely used fiber-optic sensor, has obvious advantages of compact size, high sensitivity, good reliability for long-term sensing and long-distance transmission, immunity to electromagnetic interference, and multiplexing capabilities in comparison with the conventional measurement devices (Grattan and Sun 2000; Yin et al. 2007). The scientific principle of FBG as a sensor for measuring strain or temperature has been presented before (Hill and Meltz 1997) and well understood. Details are not repeated here. The basic equation for measuring strain or temperature is

$$\frac{\Delta\lambda_B}{\lambda_{B0}} = C_\varepsilon \Delta\varepsilon + C_T \Delta T \tag{3}$$

where λ_{B0} = the Bragg wavelength at the initial state (m); $\Delta\lambda_B$ = the wavelength shift (m) induced by strain change $\Delta\varepsilon$ and temperature variation ΔT (°C); and C_ε and C_T = coefficients corresponding to strain and temperature with typical values of 0.78 and 6.67×10^{-6}/°C, respectively.

Working Principle of a Novel FBG-Based Effective Stress Cell

In the design of the effective stress cell, a circular stainless-steel plate (one diaphragm) with 1 mm thickness is used as a sensing plate. It is assumed that the pressure is uniformly exerted over the whole area of the sensing plate. According to the thin plate theory (Timoshenko and Woinowsky-Krieger 1959), when a circular thin plate with fixed boundaries is subjected to a uniform pressure, the magnitude of deflection induced at a certain radial distance from the center of the plate is calculated as

$$\omega = \frac{3p(1-\upsilon^2)}{16Eh^3}(a^2 - r^2)^2 \tag{4a}$$

where ω = the induced deflection (m); p = the applied uniform pressure (Pa); υ = Poisson's ratio; E = elastic modulus of the plate material (Pa); h = the thickness of the circular plate (m); a = the radius of the plate (m); and r = the radial distance from the center of the plate. Denoting $D = Eh^3/12(1-\upsilon^2)$ as bending stiffness of the plate (N·m), the deflection is rewritten as

$$\omega = \frac{p}{64D}(a^2 - r^2)^2 \tag{4b}$$

The strain in radial direction (Timoshenko and Woinowsky-Krieger 1959) is

$$\varepsilon_r = -z\frac{d^2\omega}{dr^2} = z\frac{p}{16D}(a^2 - 3r^2) \tag{5}$$

where ε_r = the radial strain at r, z is the distance from the neutral axis of the plate (m). If an FBG sensor is adhered on the back surface ($z = h/2$) and at the center ($r = 0$) of the plate, the FBG sensor measures the maximum strain which is obtained by

$$\varepsilon_{r,\max} = \varepsilon_{r,r=0} = \frac{h}{2}\frac{p}{16D}a^2 = \frac{p}{32D}ha^2 \tag{6}$$

Substituting Eq. (6) into Eq. (3), noting $\Delta\varepsilon = \varepsilon_{r,\max}$, the relationship of the shift in Bragg wavelength and applied pressure is given as

$$\frac{\Delta\lambda_B}{\lambda_{B0}} = C_\varepsilon \frac{p}{32D}ha^2 + C_T\Delta T \tag{7}$$

The temperature change ΔT can be measured separately. In the physical model test in our laboratory, a constant temperature of 20°C was kept so that ΔT was zero. Thus Eq. (7) is simplified as

$$\frac{\Delta\lambda_B}{\lambda_{B0}} = C_\varepsilon \frac{p}{32D}ha^2 \tag{8}$$

Hence, the shift in Bragg wavelength is proportional to the applied pressure p.

Design of a Novel FBG-Based Effective Stress Cell

Fig. 1(c) shows the design of a novel FBG-based effective stress cell. The effective stress cell consists of (1) a thin plate as a "sensing plate" in the front for contacting soil particles, (2) a "perforated disc base" on the back of the cell, and (3) an FBG sensor (FBG 1) is adhered at the back center of the "sensing plate." If necessary, another FBG sensor (FBG 2) can be placed inside the cell without contacting the "sensing plate" to measure temperature change for temperature compensation. Both the "sensing plate" and the "perforated disc base" are fixed on a very stiff circular "rigid ring" by full welding. In practical applications, a filter stone/paper covering the perforated disc was used to prevent the perforated disc from becoming clogged with soil particles.

The important role of the "perforated disc base" in the back is to allow pore-water to enter the space between the "sensing plate" and the "perforated disc base" and transmit pore-water pressure to the back surface of the "sensing plate." For the front surface of the "sensing plate," it is subjected to both the pore-water pressure and the "average value" of all vertical (normal) fractions of particle contact forces over the "sensing plate." It is noted that the pore-water pressures on the front surface and back surface of the "sensing plate" have the same magnitude and they are fully balanced so that the pore-water pressure in saturated soils will not cause any deflection of the "sensing plate." The deflection of the "sensing plate" is caused by the "average value" of all vertical (normal) fractions of particle contact forces only. This "average value" of all vertical (normal) fractions of particle contact forces is effective stress σ'. Considering the new design in Fig. 1(c), Eq. (8) can be written as

$$\sigma' = p = \frac{32D}{C_\epsilon h a^2}\frac{\Delta\lambda_B}{\lambda_{B0}} = \frac{32D}{C_\epsilon h a^2 \lambda_{B0}}\Delta\lambda_B \tag{9}$$

Eq. (9) is used to measure the effective stress directly.

In this study, the external diameter and total thickness of the effective stress cell are 120 and 16 mm, respectively. As depicted in Fig. 2(a), the thin "sensing plate" in disc groove is 100 mm in diameter and 1 mm in thickness. The "perforated disc base" is 120 mm in diameter and 2 mm in thickness. All parts were made of 316 stainless steel which has an elastic modulus of 193 GPa, Poisson's ratio of 0.3, and a yield strain of ±0.00105. Substituting all the values into Eq. (6), the maximum pressure p of the FBG-based effective stress cell is 201.9 kPa. A 10 mm-long FBG sensor with a central wavelength λ_{B0} of 1,542 nm was attached to the center of inner surface of the thin "sensing plate" and well protected by epoxy adhesives. In consideration of multiplexing, the FBG sensor was connected with a two-core single mode transmission fiber at both its input and output ends by using an arc fusion splicer, illustrated in Fig. 2(c).

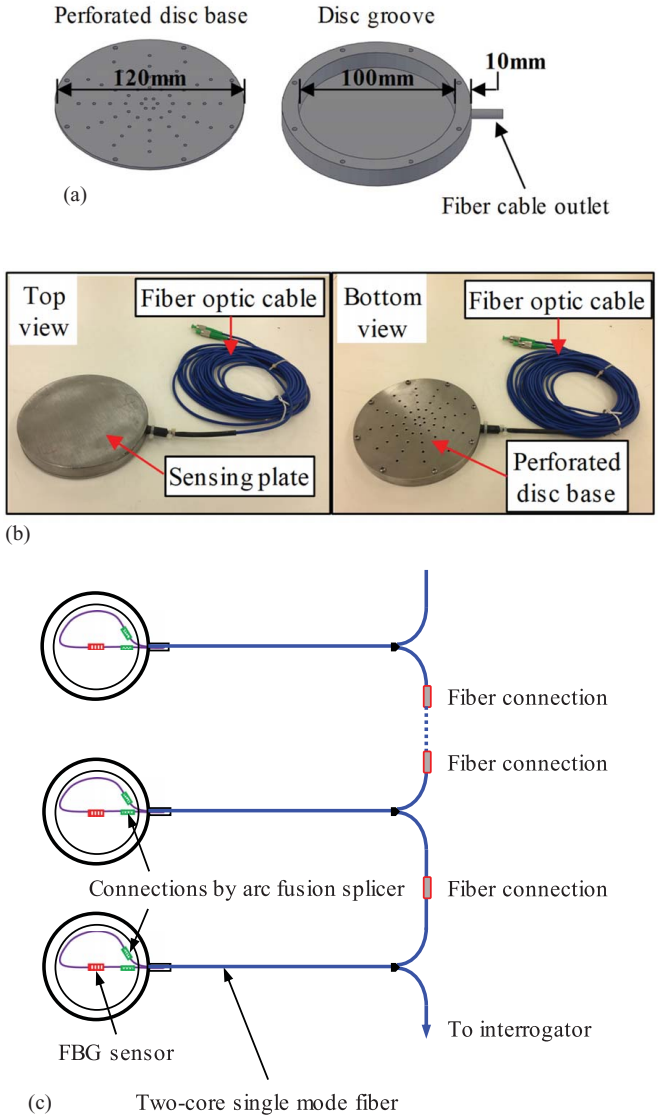

Fig. 2. Design of the FBG-based effective stress cell: (a) schematic diagram; (b) photographs; and (c) multiplexing.

Calibration of the FBG-Based Effective Stress Cell

In previous studies, calibration tests of soil pressure transducers were mostly conducted by employing gas (Correia et al. 2009), water (Dave and Dasaka 2013), oil (Zhou et al. 2006), or sand (Li et al. 2013) as the loading medium. In this study, the FBG-based effective stress cell was calibrated by applying water pressure with the perforated disk base temporarily replaced by an "impermeable stainless-steel disk" in a water container. When an "impermeable stainless-steel disk" was employed to replace the perforated disc base in the calibration tests, the groove and the "impermeable stainless-steel disk" were fitted together and sealed by an O-ring so that no water could enter the cell inside. The FBG-based effective stress cell with an "impermeable stainless-steel disk" was placed in a water container with 300 mm in diameter and 500 mm in height with a watertight cover. A GDS pressure controller was used to provide a stable water pressure with a resolution of 1 kPa and a pressure range from 0 to 2,000 kPa. In addition, the optical fiber was connected to an FBG interrogator to take readings. In order to evaluate the repeatability of the FBG-based effective stress cell and obtain a more accurate value of the calibration coefficient, two cycles including loading and unloading were performed. Furthermore, a calibration test of the FBG-based effective stress cell in its actual configuration with the perforated disc was carried out to verify the function of the FBG-based effective stress cell.

In the calibration tests, the water pressure in the range of 0–200 kPa at 20 kPa increments was applied. Fig. 3 shows calibration results for both loading and unloading. The results of two loading–unloading cycles show that the designed FBG-based effective stress cell has a good repeatability. Furthermore, a linear relationship between the reflected Bragg wavelength and applied water pressure is observed. The reflected Bragg wavelength rises from 1,541.96 to 1,542.58 nm with an increased water pressure from 0 to 200 kPa. By adopting the least-squares method, a linear transfer

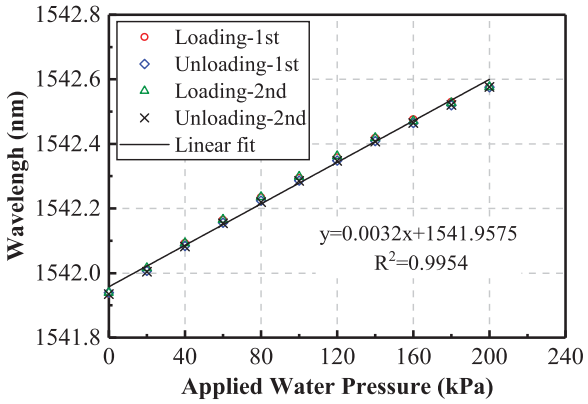

Fig. 3. Results of calibration tests on an FBG-based effective stress cell with the perforated disk temporarily replaced by an "impermeable stainless-steel disk" in a water container.

function with a good coefficient of determination (COD) value of 0.9954 is obtained and shown in Fig. 3. It is found that the slope (slope $= \Delta\lambda_B/p$) in Fig. 3 is 0.0032 nm/kPa, and the pressure resolution of this effective stress cell is 0.31 kPa when the FBG sensor is interrogated by the optical sensing interrogator (SM125) which has a wavelength resolution of 0.001 nm (i.e., 1 p.m.). According to Eq. (6), the calculated slope (slope $= \Delta\lambda_B/p$) is 0.0053 nm/kPa, larger than the measured value of 0.0032 nm/kPa. There are two main reasons: (1) the strain measured by the FBG sensor was an average strain within a FBG sensor length of 10 mm; while the strain in Eq. (6) is the maximum strain at the center ($r = 0$) and (2) the adhesive strength and thickness of epoxy adhesives increased the bending stiffness of the "sensing plate" which decreased the strain under the same applied pressure. The measured slope is more reliable. The calibrated coefficient is $p/\Delta\lambda_B = 1/0.0032 = 312.5$ (kPa/nm). Moreover, when the FBG-based effective stress cell in its actual configuration with the perforated disc was calibrated, it was found that no water pressure was measured by the FBG sensor during the test.

Verification of the FBG-Based Effective Stress Cell in a Physical Model Test

Test Setup

A physical model test was carried out to verify the workability and accuracy of the FBG-based effective stress cell in a large physical model shown in Figs. 4 and 5. The internal dimensions of the physical model are 1,000 mm in length, 600 mm in width, and 800 mm in height. There is a rubber membrane fixed on the inner surface of the top cover as shown in Fig. 4. A pressure regulator was utilized to control water pressure inside the rubber membrane so that the vertical pressure on a saturated soil inside the physical model could be controlled. The inner surface of the physical model was lined with a smooth stainless-steel sheet. Lubricating oil was spread on the stainless-steel sheet and a flexible plastic film was used to cover the steel sheet, thereby reducing the friction between the soil and the sidewalls of the physical model.

In order to monitor the applied pressure provided by rubber membrane, a conventional pore-water pressure transducer (PPT2) was mounted on the top cover of the physical model. The newly developed FBG-based effective stress cell was embedded in a fully saturated Completely Decomposed Granite (CDG) soil, which is a

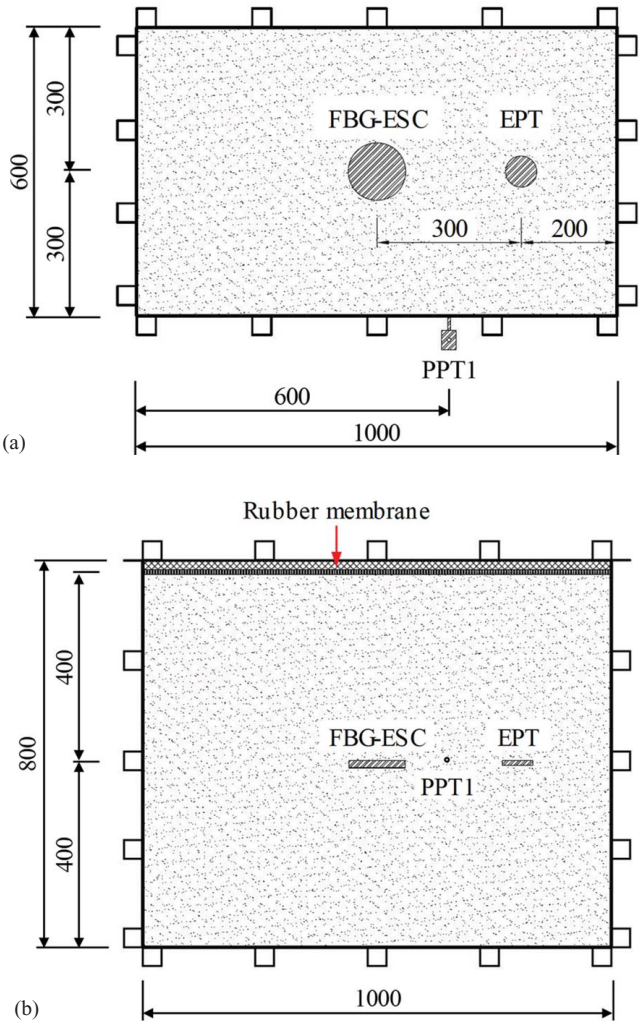

Fig. 4. The arrangement of the FBG-based effective stress cell (FBG-ESC) and the conventional earth pressure transducer (EPT) and pore-water pressure transducer (PPT1) in the physical model test: (a) top plan view (600 mm wide and 1,000 mm long); and (b) side view (830 mm high and 1,000 mm long) (unit in mm).

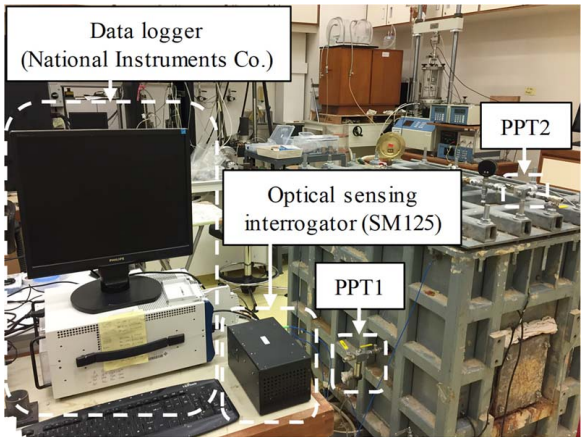

Fig. 5. Photo of the physical model test setup for validation of the new FBG-based effective stress cell (FBG-ESC).

typical soil in Hong Kong (Borana et al. 2016a, b; Lu et al. 2018), at a depth of 400 mm, together with a conventional earth pressure transducer (EPT), and a conventional pore-water pressure transducer (PPT1) installed on the sidewall of the large container at the same level as shown in Figs. 4 and 5. The CDG soil consists of 6.9% gravel, 45.2% sand, 30.5% silt, and 17.4% clay. EPT, PPT1, and PPT 2 were all calibrated in a sealed Perspex cylinder with water pressure. During the test, the FBG sensor was interrogated by the optical sensing interrogator (SM125), while data of conventional transducers were acquired by an NI data logger shown in Fig. 5.

Test Results and Discussions

A preparation stage with an average overburden pressure of 30 kPa imposed on the top of soil was performed first. This pressure of 30 kPa was held for 700 h to establish (1) the contact pressure between the rubber membrane and the top soil surface and (2) the contact of all cells with surrounding soils. After 700 h, the pressure of water in the rubber membrane was unloaded to zero and then increased to 100 kPa. The test results, including the applied pressure, total stress, and pore-water pressure measured by the conventional transducers (PPT2, EPT, and PPT1), under the average overburden pressures of 30 and 100 kPa are shown in Figs. 6(a) and 7(a) respectively. In preparation stage, due to the instability of inlet pressure from water supply and consolidation settlement of the saturated soil, the applied overburden pressure was fluctuant during the test. It is seen from Figs. 6(a) and 7(a) that the measured pore-water pressure is decreased gradually due to the dissipation of excess pore-water pressure or consolidation of the soil over time.

Since the physical model test was carried out in a saturated soil, the effective stress can be calculated by subtracting the pore-water pressure from the total stress using Eq. (1*c*) as an indirect measurement method. The calculated effective stresses for the two tests are shown in Figs. 6(b) and 7(b) respectively. The effective stresses directly measured using the FBG-based effective stress cell in the two tests are also shown in Figs. 6(b) and 7(b) for comparison. It is seen from the figures that the measured effective stress increases gradually with the dissipation of excess pore-water pressure over time and is scarcely affected by the fluctuation of the applied pressure, exhibiting a good reliability of the FBG-based effective stress cell. It is seen from Fig. 6(b) that there are some differences between the measured data by the FBG-based effective stress cell and the calculated values from the measured total stress minus the measured pore-water pressure for time from 0 to about 400 h. The difference was less than 4 kPa. The discrepancy of the results given by two methods primarily was very likely caused by (i) different locations of these cells, (ii) fluctuation of the applied pressure effecting readings of the conventional transducers (EPT and PPT1), and (iii) the response time of the conventional transducers to the applied pressure were not identical. After 400 h, the measured data by the FBG-based effective stress cell are in good agreement with the calculated values. In Fig. 7(b), the measured data by the FBG-based effective stress cell are in good agreement with the calculated values for the whole loading period and the measurement error between both values is within 3 kPa, which may be related to the soil arching effect (Labuz and Theroux 2005; Han et al. 2017) and

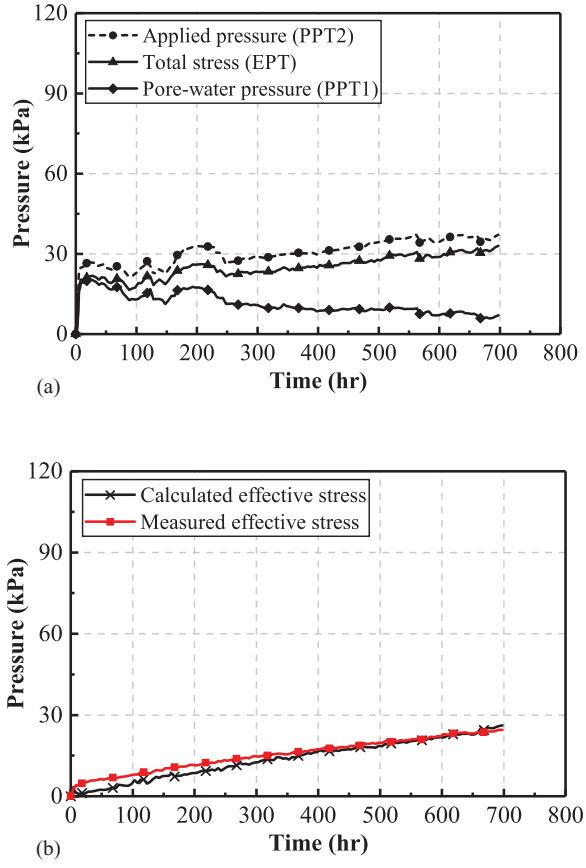

Fig. 6. Test results under the average overburden pressure of 30 kPa: (a) applied pressure, total stress, and pore-water pressure measured by the conventional transducers; and (b) comparison of calculated effective stress and effective stress measured directly.

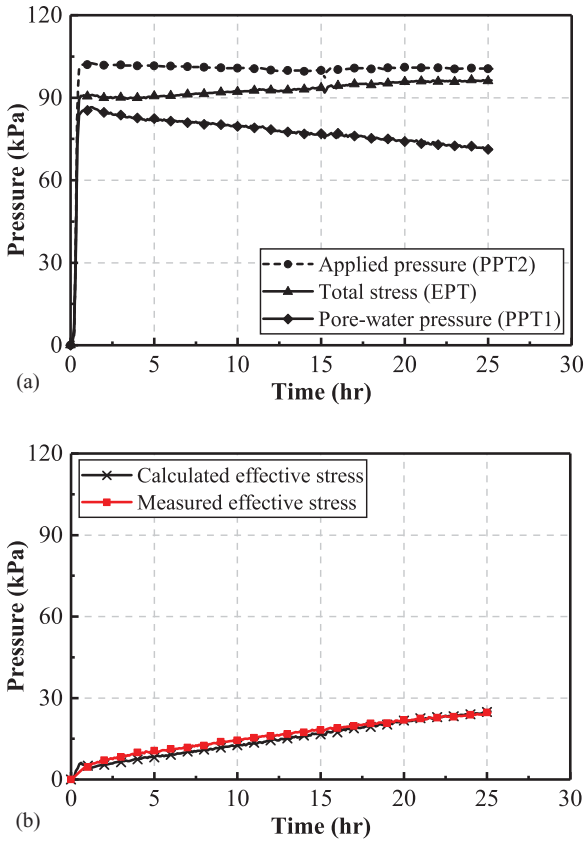

Fig. 7. Test results under the average overburden pressure of 100 kPa: (a) applied pressure, total stress, and pore-water pressure measured by the conventional transducers; and (b) comparison of calculated effective stress and effective stress measured directly.

bending stiffness of both the EPT and the effective stress cell (Wachman and Labuz 2011). In general, this newly developed FBG-based effective stress cell which can measure the effective stress in a single cell and is placed at one location can provide better and more reliable measurement of the effective stress in a saturated soil than that using the indirect measurement method using two cells at two different locations.

Summary and Conclusions

In this study, the design, calibration, and verification of a novel FBG-based effective stress cell for direct measurement of effective stress in saturated soil have been presented. The working principle of the FBG-based effective stress cell is elaborated with an equation based on the thin plate theory. The primary concept of direct measurement is that the pore-water pressures acting on both front and back surfaces of the sensing plate, which have the same magnitude, do not induce the deflection of the sensing plate and thus the measured deflection of the sensing plate is caused by the effective stress only. After replacing the perforated disc by an importable solid disc, the calibration of the FBG-based effective stress cell was conducted by employing water pressure. Moreover, one physical model test with an applied pressure of 100 kPa was conducted to examine the workability and performance of the proposed FBG-based effective stress cell. The summary and conclusions from this study are listed as follows:

1. Calibration results demonstrate that the response of the FBG-based effective stress cell to the applied pressure exhibits good linearity with high accuracy.
2. The pressure sensitivity of 0.0032 nm/kPa for the FBG-based effective stress cell can be employed in applications. When the FBG sensor is interrogated by an optical sensing interrogator with a wavelength resolution of 0.001 nm (i.e., 1 p.m.), the pressure resolution of the FBG-based effective stress cell is 0.31 kPa.
3. By comparison with the calculated effective stress values from the measured total stress and pore-water pressure provided by conventional transducers, the FBG-based effective stress cell is verified to have good accuracy for direct measurement of the effective stress in a saturated soil with high reliability.

To date, the FBG-based effective stress cell has been successfully applied in the laboratory physical model test in a saturated CDG soil which was a mix of clay, silt, and sand. In principle, the FBG-based effective stress cell can be used to measure directly the effective stress in saturated clays with low permeability. In fact, FBG-based effective stress cells will soon be placed in a large physical model to measure effective stresses in a Hong Kong marine clay. We will also consider the use of FBG-based effective stress cells to measure effective stresses in real geotechnical projects. For field applications, we will improve optical fiber cable connections, the perforated disk base, and temperature compensation for the FBG sensors.

Acknowledgments

The work in this paper is supported by an ITF project (Grant No.: ITS/049/13), a CRF project (Grant No.: PolyU 12/CRF/13E) from the Research Grants Council (RGC) of Hong Kong Special Administrative Region Government (HKSARG) of China, two GRF projects (PolyU 152796/16E, PolyU 152209/17E) from RGC of HKSARG of China. The authors also acknowledge the financial supports from the Research Institute for Sustainable Urban Development of the Hong Kong Polytechnic University and grants (1-BBAG, 1-ZVEF, 1-ZVEH, 4-BCAW, 5-ZDAF, G-YBHQ, G-YN97) from the Hong Kong Polytechnic University.

References

Borana, L., J. H. Yin, D. N. Singh, and S. K. Shukla. 2016a. "Interface behavior from suction-controlled direct shear test on completely decomposed granitic soil and steel surfaces." *Int. J. Geomech.* 16 (6): D4016008. https://doi.org/10.1061/(ASCE)GM.1943-5622.0000658.

Borana, L., J. H. Yin, D. N. Singh, S. K. Shukla, and H. F. Pei. 2016b. "Influences of initial water content and roughness on skin friction of piles using FBG technique." *Int. J. Geomech.* 17 (4): 04016097. https://doi.org/10.1061/(ASCE)GM.1943-5622.0000794.

Chang, C. C., G. Johnson, S. T. Vohra, and B. Althouse. 2000. "Development of fiber Bragg-grating-based soil pressure transducer for measuring pavement response." In *Proc. SPIE* 3986: 480–488.

Clayton, C. R. I., and A. V. D. Bica. 1993. "The design of diaphragm-type boundary total stress cells." *Géotechnique* 43 (4): 523–535. https://doi.org/10.1680/geot.1993.43.4.523.

Correia, R., J. Li, S. Staines, E. Chehura, S. W. James, J. Kutner, P. Dewhurst, P. Ferreira, and R. P. Tatam. 2009. "Fibre Bragg grating based effective soil pressure sensor for geotechnical applications." In Vol. 7503 of Proc., *20th Int. Conf. on Optical Fibre Sensors*. Bellingham, Washington: SPIE.

Dave, T. N., and S. M. Dasaka. 2013. "In-house calibration of pressure transducers and effect of material thickness." *Geomech. Eng.* 5 (1): 1–15. https://doi.org/10.12989/gae.2013.5.1.001.

Feng, W. Q., Z. Y. Liu, H. Y. Tam, and J. H. Yin. 2016. "The pore water pressure sensor based on Sagnac interferometer with polarization-maintaining photonic crystal fiber for the geotechnical engineering." *Measurement* 90: 208–214. https://doi.org/10.1016/j.measurement.2016.04.067.

Grattan, K. T. V., and T. Sun. 2000. "Fiber optic sensor technology: An overview." *Sens. Actuators, A* 82 (1–3): 40–61. https://doi.org/10.1016/S0924-4247(99)00368-4.

Han, J., F. Wang, M. Al-Naddaf, and C. Xu. 2017. "Progressive development of two-dimensional soil arching with displacement." *Int. J. Geomech.* 17 (12): 04017112. https://doi.org/10.1061/(ASCE)GM.1943-5622.0001025.

Hill, K. O., and G. Meltz. 1997. "Fiber Bragg grating technology fundamentals and overview." *J. Lightwave Technol.* 15 (8): 1263–1276. https://doi.org/10.1109/50.618320.

Labuz, J. F., and B. Theroux. 2005. "Laboratory calibration of earth pressure cells." *Geotech. Test. J.* 28 (2): 188–196. https://doi.org/10.1520/GTJ12089.

Lade, P. V., and R. De Boer. 1997. "The concept of effective stress for soil, concrete and rock." *Géotechnique* 47 (1): 61–78. https://doi.org/10.1680/geot.1997.47.1.61.

Li, F., Y. Du, W. Zhang, and F. Li. 2013. "Fiber Bragg grating soil-pressure sensor based on dual L-shaped levers." *Opt. Eng.* 52 (1): 014403. https://doi.org/10.1117/1.OE.52.1.014403.

Lu, K. K., J. H. Yin, and S. C. Lo. 2018. "Modeling small-strain behavior of Hong Kong CDG and its application to finite-element study of basement-raft footing." *Int. J. Geomech.* 18 (9): 04018104. https://doi.org/10.1061/(ASCE)GM.1943-5622.0001250.

Rojas, E., O. Chávez, and H. Arroyo. 2017. "Modeling the behavior of expansive soils using effective stresses." *Int. J. Geomech.* 17 (9): 04017062. https://doi.org/10.1061/(ASCE)GM.1943-5622.0000943.

Skempton, A. W. 1960. "Terzaghi's discovery of effective stress." In *From theory to practice in soil mechanics: Selections from the writings of Karl Terzaghi*, edited by L. Bjerrum, A. Casagrande, R. B. Peck, and A. E. Skempton, 42–53. New York: Wiley.

Talesnick, M. 2013. "Measuring soil pressure within a soil mass." *Can. Geotech. J.* 50 (7): 716–722. https://doi.org/10.1139/cgj-2012-0347.

Terzaghi, K. 1943. *Theoretical soil mechanics*. New York: John Wiley and Sons.

Timoshenko, S. P., and S. Woinowsky-Krieger. 1959. *Theory of plates and shells*. New York: McGraw-Hill.

Wachman, G. S., and J. F. Labuz. 2011. "Soil-structure interaction of an earth pressure cell." *J. Geotech. Geoenviron. Eng.* 137 (9): 843–845. https://doi.org/10.1061/(ASCE)GT.1943-5606.0000501.

Wei, H. Z., D. S. Xu, and Q. S. Meng. 2018. "A newly designed fiber-optic based earth pressure transducer with adjustable measurement range." *Sensors* 18 (4): 932. https://doi.org/10.3390/s18040932.

Yin, J. H. 2013. "Development of New FBG-based Transducers for Integrated Measurement of Total Earth Pressure, Porewater Pressure, and Effective Stress." A research and development project (ITS/049/13) funded by Innovation and Technology Fund (ITF) of the Government of the Hong Kong Special Administrative Region of China.

Yin, J. H., H. H. Zhu, W. Jin, A. T. Yeung, and L. M. Mak. 2007. "Performance evaluation of electrical strain gauges and optical fiber sensors in field soil nail pullout tests." In *Proc., HKIE Geotechnical Division Annual Seminar*, 249–254.

Zhou, W. H., F. Tan, and K. V. Yuen. 2018. "Model updating and uncertainty analysis for creep behavior of soft soil." *Comput. Geotech.* 100: 135–143. https://doi.org/10.1016/j.compgeo.2018.04.006.

Zhou, Z., H. Wang, and J. Ou. 2006. "A new kind of FBG-based soil-pressure sensor." In *Optical Fiber Sensors*. Washington, DC: Optical Society of America. https://doi.org/10.1364/ofs.2006.the90.